HHS Public Access

Author manuscript

*Matrix Biol*. Author manuscript; available in PMC 2017 April 24.

Published in final edited form as:

*Matrix Biol*. 2016 ; 52-54: 426–441. doi:10.1016/j.matbio.2016.01.004.

# One size does not fit all: developing a cell-specific niche for in vitro study of cell behavior

**Milos Marinkovic**[a,b], **Travis J. Block**[a,b], **Rubie Rakian**[a], **Qihong Li**[c], **Exing Wang**[d], **Matthew A. Reilly**[b], **David D. Dean**[a,b], and **Xiao-Dong Chen**[a,b,e]

[a]Department of Comprehensive Dentistry, University of Texas Health Science Center at San Antonio, San Antonio, TX, USA

[b]Department of Biomedical Engineering, University of Texas at San Antonio, San Antonio, TX, USA

[c]Department of Stomatology, Affiliated Hospital of the Academy of Military Medical Sciences, Beijing, China

[d]Department of Cellular and Structural Biology, University of Texas Health Science Center at San Antonio, San Antonio, TX, USA

[e]Audie Murphy VA Medical Center, San Antonio, TX, USA

## Abstract

For more than 100 years, cells and tissues have been studied in vitro using glass and plastic surfaces. Over the last 10–20 years, a great body of research has shown that cells are acutely sensitive to their local environment (extracellular matrix, ECM) which contains both chemical and physical cues that influence cell behavior. These observations suggest that modern cell culture systems, using tissue culture polystyrene (TCP) surfaces, may fail to reproduce authentic cell behavior in vitro, resulting in “artificial outcomes.” In the current study, we use bone marrow (BM)- and adipose (AD)-derived stromal cells to prepare BM-ECM and AD-ECM, which are decellularized after synthesis by the cells, to mimic the cellular niche for each of these tissues. Each ECM was characterized for its ability to affect BM- and AD-mesenchymal stem cell (MSC) proliferation, as well as proliferation of three cancer cell lines (HeLa, MCF-7, and MDA-MB-231), modulate cell spreading, and direct differentiation relative to standard TCP surfaces. We found that both ECMs promoted the proliferation of MSCs, but that this effect was enhanced when the tissue-origin of the cells matched that of the ECM (i.e. BM-ECM promoted the proliferation of BM-MSCs over AD-MSCs, and vice versa). Moreover, BM- and AD-ECM were shown to preferentially direct MSC differentiation towards either osteogenic or adipogenic lineage, respectively, suggesting that the effects of the ECM were tissue-specific. Further, each ECM influenced cell morphology (i.e. circularity), irrespective of the origin of the MSCs, lending more support to the idea that effects were tissue specific. Interestingly, unlike MSCs, these ECMs did

Correspondence to Xiao-Dong Chen: at: Department of Comprehensive Dentistry, University of Texas Health Science Center at San Antonio, 7703 Floyd Curl Drive, San Antonio, TX 78229-3900, USA. chenx4@uthscsa.edu.

Competing interests

Dr. Chen is a board member and shareholder in StemBioSys, Inc. (San Antonio, TX). All other authors have no financial or competing interests to declare.

not promote the proliferation of the cancer cells. In an effort to further understand how these three culture substrates influence cell behavior, we evaluated the chemical (protein composition) and physical properties (architecture and mechanical) of the two ECMs. While many structural proteins (e.g. collagen and fibronectin) were found at equivalent levels in both BM- and AD-ECM, the architecture (i.e. fiber orientation; surface roughness) and physical properties (storage modulus, surface energy) of each were unique. These results, demonstrating differences in cell behavior when cultured on the three different substrates (BM- and AD-ECM and TCP) with differences in chemical and physical properties, provide evidence that the two ECMs may recapitulate specific elements of the native stem cell niche for bone marrow and adipose tissues. More broadly, it could be argued that ECMs, elaborated by cells ex vivo, serve as an ideal starting point for developing tissue-specific culture environments. In contrast to TCP, which relies on the “one size fits all” paradigm, native tissue-specific ECM may be a more rational model to approach engineering 3D tissue-specific culture systems to replicate the in vivo niche. We suggest that this approach will provide more meaningful information for basic research studies of cell behavior as well as cell-based therapeutics.

### Keywords

Cell culture; Extracellular matrix; Cell microenvironment; Niche; Mesenchymal stem cells (MSCs); Differentiation

## Introduction

The origins of cell and tissue culture date to the early 1900's, with studies reported by Carrel, Burrows, and others describing the culture of mammalian tissue outside the human body [1]. Initially, tissue explants were placed on glass coverslips in a drop of hypotonic plasma that was allowed to clot before being inverted over a concave microscope slide. Considerable progress has been made over the last 100 years, including the isolation and growth of single cells [2], the seminal studies of Harry Eagle leading to the successful development of defined media [3], and the development of glow discharge treatment of tissue culture polystyrene (TCP) to facilitate cell attachment [4], that have facilitated many discoveries in modern medicine and the award of several Nobel prizes. Today, despite the achievement of many significant milestones in methods of cell and tissue culture, our studies of cell behavior continue to be constrained by an inadequate replication of the in vivo environment in culture.

An ideal tissue culture system should not only support the growth of cells in vitro but, more importantly, cause them to faithfully retain and express their in vivo phenotypic characteristics. However, because of their simplicity, TCP plates have been widely used for this purpose. Although much has been learned using such “two-dimensional” (2D) culture surfaces, it has become increasingly clear that these classical culture systems are inadequate for replicating in vivo cell behavior and studying cell and molecular biology, understanding the mechanisms of diseases, and improving diagnosis and treatment of diseases [5–7].

Within the body, cells reside in tissues that contain distinct physiological microenvironments or niches. Cells receive not only biochemical and physical cues from this local environment,

but also interact with and remodel it, by secreting extracellular matrix (ECM) proteins and growth factors that play a role in cell signaling pathways and producing proteolytic enzymes capable of modifying the ECM. This “give and take” relationship between cells and their niche has the effect of directing changes in cell behavior that include cell quiescence, migration, proliferation (symmetric or asymmetric division), differentiation, survival, and senescence [8]. Over the last decade, it has become increasingly clear that this relationship cannot be studied in classical 2D culture systems.

The local microenvironment (niche) of the cell is mainly comprised of ECM components that form a three-dimensional (3D) network which anchors cells and provide a reservoir of growth factors/cytokines that direct cell fate and function [9–11]. For this reason, we have focused on developing an authentic niche *ex vivo*, instead of optimizing growth media, for controlling the fate of mesenchymal stem cells (MSCs). With this approach, we were the first to establish a culture system using cell-free native ECM made by bone marrow stromal cells. Although this bone marrow stromal cell-derived ECM (BM-ECM) contained very few growth factors, it dramatically promoted MSC replication, retention of multipotency, and significantly increased responsiveness to differentiation stimuli when compared to MSCs cultured on TCP [12,13]. We have demonstrated that this native BM-ECM is composed of, at least in part, collagens, fibronectin, small leucine-rich proteoglycans (SLRPs), and basement membrane components [12,13]. These matrix proteins are known to play a key role in regulating cell adhesion, migration, proliferation, differentiation, and survival [14–16]. Importantly, many of these cell functions are controlled by growth factors and cytokines (TGFβ, TNFα and PDGF) that are stored in the ECM and presented to cells as they interact with and remodel the matrix. The types of control mechanisms employed include secretion of growth factors in latent form, storage in the ECM by use of specific binding proteins to prevent receptor binding, activation of latent or bound forms via proteolytic processing [17–19], and modulation of receptor activity [20,21]. Indeed, our previously published studies have shown that ECM proteins regulate MSC behavior by modulating both endogenous (stem cell-derived) and exogenous (externally added or serum-derived) growth factor stores [10,12,14,22].

To extend these observations, we hypothesized that native ECM, replicated *ex vivo* by this technology, contains a unique collection of key effective components (or cues) that direct MSC differentiation to the cell lineage that originally synthesized the ECM. In the current study, we tested this hypothesis by investigating whether BM-ECM was unique in its ability to preserve MSC properties by comparing it to ECM produced in a similar fashion by adipose tissue-derived stromal cells. We compared the response of bone marrow- or a d ipose-derived MSCs (BM-MS Cs, o r AD-MSCs, respectively), as well as cancer cell lines, to culture on the same substrates including BM-ECM, adipose-derived ECM (AD-ECM), and TCP. We also characterized the biomolecular composition, architectural and mechanical properties of BM-ECM versus AD-ECM in an effort to identify physical and chemical cues that may uniquely characterize the ECM present in the bone marrow and adipose-tissue microenvironments. The results provide evidence that cells are extremely sensitive to their culture substrate and raise questions/concerns regarding both potential inherent bias and the reliability of results obtained with cells maintained on the classical 2D culture system (TCP).

## Results

### Proliferation of bone marrow- and adipose-derived MSCs, but not cervical or breast cancer cells, is increased by culture on tissue-specific ECMs

Bone marrow-derived BM-MSCs and adipose-derived MSCs (AD-MSCs) were cultured for 4 days on TCP and two types of ECMs, bone marrow-derived ECM (BM-ECM) and adipose-derived ECM (AD-ECM) (Fig. 1A). Compared to TCP, BM-MSC proliferation was significantly increased by >2-fold with culture on the two ECMs (i.e. BM-ECM and AD-ECM). Similarly, AD-MSCs displayed higher levels of proliferation on the ECMs (1.4- to 2.0-fold) than TCP. Interestingly, the degree of enhancement on the ECMs was *tissue-specific*. That is, BM-MSCs achieved the highest cell number on BM-ECM, while AD-MSCs displayed the highest cell number on AD-ECM.

The expression of stem cell markers (CD73, CD90, CD105, CD146, SSEA-4) was largely retained after culture on all three substrates (data not shown). After 4 and 7 days, BM-MSCs showed a uniformly high (≥ 90%) expression of all markers on both ECMs and TCP, while AD-MSCs only displayed this high level of expression for CD73, CD90, and CD105. With continued culture, for up to 14 days, there were varying degrees of loss of marker expression with the greatest loss occurring on TCP. CD73, CD90 and CD105 were maintained at relatively high levels during the second week of culture, while expression of CD146 a nd SSEA-4 was further reduced by 50%-80% for both BM- and AD-MSCs on TCP.

We next examined whether the ECMs promoted the proliferation of cancer cells, such as the cervical cancer cell line, HeLa, and the breast cancer cell lines, MDA-MB-231 (estrogen receptor [ER] negative) and MCF-7 (ER positive) (Fig. 1B). Unlike the effect observed with MSCs, both ECMs failed to stimulate proliferation after 4 days in culture compared to TCP. HeLa cell proliferation was significantly reduced on both ECMs. The greatest reduction was found on AD-ECM, which was not only significant versus TCP, but BM-ECM as well. A similar inhibitory trend was observed with MCF-7 cells, but the only significant reduction was found with AD-ECM. Interestingly, MDA-MB-231 cells grew equally well on TCP and AD-ECM, while growth on BM-ECM was inhibited slightly.

### Tissue-specific ECMs affect MSC morphology and direct MSC differentiation

MSC morphology, after culture on TCP or the two ECMs, was evaluated by measuring cell circularity as an index of cell spreading (Fig. 2). Surprisingly, both BM- and AD-MSCs exhibited similar morphological trends (i.e. cell circularities), when cultured on the three surfaces. Cells cultured on BM-ECM adopted a narrow, spindle-like shape, with low cell circularity, while those maintained on AD-ECM were more circular in shape. Cells grown on TCP had circularity values that were intermediate between those of cells grown on the two ECMs.

Since cell morphology and cytoskeletal organization have been linked to intracellular signaling and cell fate, we evaluated the tissue-specific ability of the ECM to direct MSC differentiation (Fig. 3). BM-MSCs were cultured to confluence on TCP, BM-ECM, and AD-ECM, followed by a media exchange to either osteoblast or adipocyte induction media, and the cultures continued for an additional 3 or 2 weeks, respectively. Cultures treated with

osteoblast induction media were stained with Alizarin Red to visualize calcium deposition, while those treated with adipocyte induction media were stained with Oil Red O to visualize lipids (Fig. 3A). The results clearly showed the presence of more calcium deposition in cultures on BM-ECM (versus AD-ECM or TCP) and more lipid droplets present in cultures maintained on AD-ECM (versus BM-ECM or TCP). Quantitation of pixel staining further confirmed the visual observations (Fig. 3B).

### Analysis of similarities and differences in BM-versus AD-ECM protein composition

ECM protein composition was analyzed using mass spectrometry (MS). BM- and AD-ECM shared approximately 64% of their protein components. From the collagen family, the most frequently found members were collagen type VI, followed by types XII and I. Further, there was little difference in the amount of these collagens found in both ECMs and, interestingly, type VI collagen comprised more than 70% of the collagen content in both ECMs (Fig. 4A). Proteoglycans and glycoproteins were a major source of compositional variation between the two ECMs (Fig. 4B). Both BM- and AD-ECM contained considerable amounts of heparan sulfate proteoglycans (biglycan and fibulin). However, BM-ECM appears to be richer in galectins, while AD-ECM uniquely contains decorin and lumican.

### Architecture of BM- and AD-ECMs is strikingly different

We employed several imaging modalities to evaluate each ECM (Fig. 5). Second-harmonic generation (SHG) microscopy provided information on the fibrillar collagenous structure of the ECM (Fig. 5, left); in BM-ECM, the matrix contained discrete fibrils that were evenly spaced and directionally oriented, while in AD-ECM, the fibrils were more diffuse and randomly distributed. We next employed immunohistochemical staining to identify structural motifs in the ECM that are contributed by specific biochemical components. Due to its abundance in both ECMs, as demonstrated by the protein analysis described above, collagen VI was selected as a target for immunofluorescence microscopy (Fig. 5, center). With this approach, BM-ECM was characterized by fine, highly aligned collagen VI fibrils, while AD-ECM contained fibrils that were less ordered than those in BM-ECM and organized into denser bundles. Taken together with data obtained using SHG microscopy, it was concluded that these two ECMs exhibited unique architectures that were chiefly attributable to variations in collagen VI organization.

### Topographical and mechanical properties of BM- and AD-ECMs are unique

Atomic force microscopy (AFM) was used to characterize the topographical features of the ECMs (Fig. 5, right). Surface mapping indicated that the ECMs had structural features similar to those observed using SHG microscopy and immunofluorescence microscopy (see above). Collagen fibers in BM-ECM were more aligned than those in AD-ECM and displayed parallel patterns in all three imaging techniques (Fig. 6). Topographically, BM-ECM was significantly rougher and had a higher mean surface roughness ($R_a$) (Fig. 7) and maximum height ($R_z$) (data not shown) than AD-ECM.

Mechanical characterization of the two types of ECM was performed using small angle oscillatory shear (SAOS) rheology. BM- and AD-ECM were distinguished by a significant difference in mechanical stiffness (Fig. 8). The storage moduli of BM- and AD-ECM

differed by three orders of magnitude, with BM-ECM providing a significantly more stiff culture substrate than AD-ECM. The considerable difference in mechanical stiffness between BM- and AD-ECM may play an important role in regulating cell behavior and defining these two distinct microenvironments.

### Contact angle and surface energy of BM- and AD-ECMs are distinct and differ markedly with TCP

Next, aqueous wetting of each of the ECMs was evaluated using contact angle analysis. The contact angle formed by water on TCP and the two ECMs was measured to provide a relative measure of hydrophobicity (high contact angle) and hydrophilicity (low contact angle) for each. The surfaces produced a broad range of aqueous contact angles in the order: TCP > BM-ECM > AD-ECM (Fig. 9A).The results indicated that TCP (57 °) was considerably more hydrophobic than the two ECMs. Among the ECMs, BM-ECM produced a significantly larger contact angle (36 °) than AD-ECM (7 °), suggesting that it was relatively more hydrophobic.

The surface energy of BM- and AD-ECMs was determined using the Oss–Chaudhury–Good method [23]. In addition to aqueous wettability, noted above, contact angle measurements for glycerol and toluene were measured on both types of ECMs (Fig. 9A) to compute the total surface free energy. BM- and AD-ECMs were found to display distinct surface free energies (Fig. 9B).

## Discussion

In vitro tissue culture systems for studying cell behavior have been under development and continual refinement since the late 19th century. For the most part, these efforts have focused on optimizing the growth media rather than the culture surface or substrate [24,25]. Recently, this focus has changed and attempts to generate a 3D matrix have employed type I collagen gels or Matrigel™, a mixture primarily containing laminin, collagen type IV, and heparan sulfate proteoglycans. There is little dispute that a 3D matrix is more physiologically relevant for culturing MSCs than traditional 2D culture systems using TCP. However, the results reported here indicate that it may be time to expand the paradigm to include 3D matrices that are more natural and “tissue-specific” rather than simply prepared from a single component (e.g. polylactic acid scaffolds or various nanomaterials) or purified matrix proteins (e.g. type I collagen or fibronectin).

MSCs can differentiate into many distinct cell lineages. The direction of MSC differentiation is controlled by the tissue-specific niche that is mainly comprised of ECM proteins and associated growth factors. It is very doubtful that the intricate and highly ordered nature of the niche can be reproduced with synthetic or purified components. In an effort to reconstitute the MSC niche in vitro, we previously described a cell-assembled ECM that recapitulates the native microenvironment and dramatically promotes MSC replication and facilitates the retention of their multipotency [12,26,27].

In the present study, we investigated whether such native ECM generated by our method was unique in its ability to preserve MSC properties by comparing it to ECM assembled by

adipose tissue-derived stromal cells. Our working hypothesis is that the ECM generated by these different types of stromal cells can replicate the key effective components necessary to influence the proliferation and differentiation of MSCs into the lineage of the cells that synthesized the original ECM (i.e. stromal cells of the same lineage).

Initially, we compared the proliferation of BM-MSCs and AD-MSCs cultured on TCP, BM-ECM or AD-ECM. Interestingly, the results showed that both BM-MSCs and AD-MSCs proliferated to a greater extent on the ECM synthesized by stromal cells derived from the corresponding tissue (Fig. 1A). In our studies of spreading morphology, we noted that both types of MSCs cultured on BM-ECM displayed a high degree of spreading and a spindle-like morphology, while cells on AD-ECM showed reduced spreading and a rounded shape (Fig. 2). Analysis of differentiation efficiency showed that BM-ECM more efficiently promoted osteogenic (versus adipogenic) differentiation, while AD-ECM exerted the reciprocal effect (Fig. 3). These findings are consistent with reports by others showing that changes in morphology (shape/spreading) are associated with osteoblast or adipocyte differentiation [28–32].

Due to similarities in proliferation of stem cells and cancer cells, we compared the proliferation of three types of cancer cells ( HeLa, MCF7 and MDA-MB-231) grown on TCP, BM-ECM and AD-ECM. Unlike the MSCs, neither BM-ECM nor AD-ECM promoted the proliferation of the cancer cells, indicating that the same environmental cues had different effects on various types of cells (Fig. 1B). More interestingly, we found that these native ECMs suppressed proliferation of the cancer cells as trypan blue staining revealed that > 90% of the cells were viable and not undergoing apoptosis. Although the underlying mechanisms behind this effect remain to be investigated, it suggests that cancer cells may require their own specific niche. Recently, studies supporting this assertion have shown that tumors synthesize an ECM that is stiffer than that of the surrounding healthy tissue [33,34].

To further determine the essential differences between BM-ECM and AD-ECM responsible for directing MSC behavior, we analyzed the biomolecular composition and architecture of the two ECMs. Mass spectrometry (MS) indicated the presence of three main collagen types with a very similar pattern of abundance in both BM-ECM and AD-ECM (Fig. 4A). Analysis of all proteins present showed that the two ECMs contained approximately 64% of the same components (Fig. 4B). The most significant differences in protein composition between the two ECMs were attributed to members of the small-leucine rich proteoglycan (SLRP) family (Fig. 4B). Since SLRPs play a critical role in organizing the collagen network [35,36], different ratios of decorin or biglycan to the various collagens present in BM-ECM versus AD-ECM may contribute to the synthesis (or assembly) of each ECM's unique architecture. It has been reported that decorin associates with all collagens found in the ECM and participates in type I collagen fibrillogenesis [37–40] and the assembly of type VI [41–43] and type XII [44,45] collagens. Further, biglycan is involved in the organization of collagen types I [46–48] and VI [42,43]. In addition to their role in directing collagen architecture, SLRPs play a modulatory role in stem cell fate by sequestering transforming growth factor-β (TGF-β) within the ECM [10,14]. Given their broad involvement in both the physical assembly of the ECM and signaling pathways that determine cell-fate, SLRPs may hold the key to understanding both tissue-specific microenvironments in the body and

recapitulating their properties in stem cell culture (for a comprehensive review of the role of proteoglycans in regulating cell fate and other functions, see Iozzo and Schaeffer, 2015) [49].

Although BM-ECM and AD-ECM did not exhibit dramatic differences in collagen composition, the collagens in each ECM are organized differently and assembled in unique patterns (Fig. 5). BM-ECM displayed directionally organized fibrillar collagens, while AD-ECM showed a more randomly organized fibrillar matrix (Fig. 6). Based on the results of the protein analyses discussed above and immunofluorescent (IF) staining, type VI collagen may be one of the principle collagenous components involved in creating the two ECM architectures. In addition, there is accumulating evidence that type VI collagen may play a role in directing stem cell fate. Andersen et al. (2011) reported a shift in the immunolocalization of type VI collagen with MSC differentiation. In undifferentiated cells, type VI collagen was localized exclusively to the cytoplasm. In contrast, when the media were changed to stimulate osteogenesis or adipogenesis, type VI collagen was found localized to the cell membrane and pericellular matrix [50]. More recently, Urciuolo et al. (2013) demonstrated that type VI collagen plays a key role in creating the muscle satellite cell niche. In their study, type VI collagen knock-out mice were found to have reduced muscle regeneration capacity, decreased muscle stiffness, and impaired satellite cell self-renewal [51]. When wild type fibroblasts were engrafted to restore collagen production, the mechanical properties of the tissue and satellite cell function returned to near normal. These observations, implicating an important role for collagen VI in directing stem cell behavior, provide additional support for the hypothesis that BM- and AD-ECM replicate critical components of the in vivo MSC microenvironment.

When differences in ECM architecture and compositional data for SLRP proteoglycans (above) are considered together, it's possible that tissue-specific ratios of biglycan or decorin-to-collagen type VI in the two ECMs may provide a rational basis for explaining how these two unique architectures are assembled by the cells. In previous studies, it has been shown that biglycan plays a role in organizing type VI collagen into hexagonal patterns and with increased biglycan to collagen VI molar ratio an increased collagen network surface area [43]. Similarly, we observed that while overall collagen type VI content did not vary significantly between BM- and AD-ECM, biglycan content was considerably higher in the adipose-derived matrix. It is possible that differences between BM-ECM (with its highly-ordered, fibrous network) and AD-ECM (with more random, web-like structure) are due to differences in the ratio of biglycan to collagen type VI (Figs. 5, 6). If further studies confirm that the ratio of biglycan to collagen type VI is important in the assembly of these two matrices, it suggests that SLRPs may also play a role in creating the topographical and mechanical differences that characterize each of these two ECMs.

Physical properties recognized as a source of variation among the ECMs have been shown in numerous studies to affect processes critical to cell survival and fate. While both ECMs were characterized by significantly greater topographical variation than TCP, BM-ECM was rougher than AD-ECM (Fig. 7). Culture substrate topography has been reported to influence protein adsorption and cell adhesion, spreading, alignment, and motility [52,53]. Further, topography has been shown to affect stem cell proliferation and differentiation [54–58]. As

such, the topographical differences between the two ECMs may have also contributed to the observed differences in MSC behavior.

It is known that substrate mechanical stiffness has a significant effect on differentiation; more compliant surfaces favor the adipogenic lineage, while stiffer surfaces favor osteogenesis [59–61]. We found that BM-ECM was three orders of magnitude stiffer than AD-ECM (Fig. 8). While the mechanical properties of the two ECMs approximated those of other tissue--specific matrices [62,63], TCP stiffness, in the range of 3 gigapascals (GPa) [64], far exceeds that of any known tissue, collagenous matrix, or tissue engineering scaffold. Relative to TCP, the tissue-specific effects of these ECMs on MSC proliferation and differentiation may reflect the ability of the two ECMs to recapitulate the physical characteristics of the MSC niches found in bone marrow and adipose tissue.

Since substrate surface energy also has the potential to influence MSC spreading morphology and cytoskeletal organization by affecting protein adsorption to the culture surface and cell interactions [65–68], we measured the aqueous wetting behavior of TCP and the two ECMs and found considerable differences in hydrophobicity between the three surfaces (Fig. 9A). For cell culture substrates, a certain degree of hydrophobicity is required in order to facilitate protein adsorption from the media and cell attachment. However, due to the excessive hydrophobicity of polystyrene, TCP is treated with oxygen-containing groups to render the surface more hydrophilic [4,24]. Both ECMs were substantially more hydrophilic than even the treated TCP and produced significantly lower aqueous contact angles (Fig. 9A). Next, we applied the Oss–Chaudhury–Good method and showed that the two ECMs had a significantly higher surface free energy than TCP. Interestingly, the ECMs displayed surface free energies (Fig 9B) higher than many synthetic polymers commonly used as culture substrates or tissue engineering scaffold materials [69–72]. As culture substrates/scaffolds are often designed to favor various types of electro-static interactions that influence protein/solute adsorption and ultimately modulate cell attachment, spreading, and differentiation [32,55,58,66– 68,73,74], it is likely that the observed differences in surface energy between TCP, BM- and AD-ECM play a role in determining stem cell fate when cultured on these substrates.

In summary, the present study provides evidence indicating that native ECM (BM-ECM and AD-ECM), produced *ex vivo*, replicated the tissue-specific microenvironment (niche) of BM-MSCs and AD-MSCs. Although further research is required to confirm whether the ratio of SLRP (e.g. biglycan and decorin) to collagen plays a significant role in producing the unique architectures and distinct physical/mechanical properties displayed by the two ECMs, we hope that the knowledge gleaned from the present study can serve as a starting point for the development of more sophisticated culture systems that replicate the in vivo niche. These advanced culture systems will provide tissue-specific environments for studying cell behavior in response to new drugs such as new radio- and chemo-therapeutics for cancer patients. Finally, the establishment of more sophisticated tissue-specific 3D scaffolds, fabricated using synthetic materials coated with tissue-specific ECM and supplied with an appropriate combination of growth factors, may allow us to more efficiently control MSC fate for basic research as well as cell-based therapies.

## Materials and methods

### Preparation of BM- and AD-MSCs

Freshly isolated human bone marrow mononuclear cells (20–25 year old donors), containing BM-MSCs, were obtained from Lonza Group Ltd. (Walkersville, MD). Viability was consistently greater than 98% by trypan blue exclusion. Primary cells were seeded ($3 \times 10^5$ cells/cm $^2$) into standard 6 well tissue culture plates (Sigma-Aldrich, St. Louis, MO) and cultured in "growth media" consisting of α-MEM (Life Technologies, Grand Island, NY) containing glutamine (2 mM), penicillin/streptomycin, and 15% fetal bovine serum (FBS) (Atlanta Biologicals, Lawrenceville, GA) [pre-selected for growth enhancing activity]. Half-volume media changes were performed every 3–4 days and the cultures continued for 2–3 weeks until 70–80% confluence was achieved. Non-adherent cells were removed by washing with phosphate buffered saline (PBS) and adherent cells (passage 1; P1 cells) collected after trypsinization. The MSC phenotype was confirmed by high expression of CD73, CD90, and CD105.

AD-MSCs were obtained from Lonza Group Ltd. (Walkersville, MD) for preparation of AD-ECM and study of their behavior.

### Preparation of cell-free BM- and AD-ECM

BM- and AD-ECM were produced under aseptic conditions using procedures developed by our lab and previously described [12]. Briefly, BM- and AD-MSCs, isolated as described above, were seeded into 6 well tissue culture plates at $6 \times 10^3$ cells/cm $^2$ and cultured in "growth media" for 15 days with media changes every 3–4 days. During the last 8 days of culture, ascorbic acid (50 μM) (Sigma-Aldrich, St. Louis, MO) was added to the media. The resulting ECM was washed with PBS and decellularized by incubation for 5 min at 37 °C in PBS containing 0.5% Triton X-100 and 20 mM $NH_4OH$. The decellularized ECM was washed 3 times with PBS, followed by 3 sterile distilled water rinses, and then used in the experiments immediately or allowed to dry at room temperature before storing in 4 °C. If dried before use, the ECM was re-hydrated for 1 h at 37 °C with PBS, the PBS removed, and experimental media added. No measureable differences have been observed between freshly prepared and dehydrated/ re-hydrated ECMs. Upon rehydration, the ECMs in each well swell to a thin gel, while maintaining their characteristic architecture [12,13]. The described procedure results in the production of a reproducible culture surface (for an individual donor) that has been used in our lab for the last 8 years. The current study employed ECMs produced by MSCs from multiple donors (> 20) over the last 4 years.

Overall, ECM quality is controlled through use of well-characterized mononuclear cells (MNCs) and standardized initial cell seeding densities, culture times, and decellularization methods to extract the cells. BM-MSCs are obtained from freshly isolated MNCs, procured from 20 to 23-year old donors, whose cell surface markers are characterized by FACS analysis before establishing primary cell cultures. After two passages of cell expansion, sufficient numbers of cells are obtained for producing a large-scale number of ECMs using an appropriate cell seeding density (< 6000 cells/cm $^2$). Seeding densities are standardized, by determining cell doubling time for each batch, so that the cultures reach confluence at

day 7. Each batch of ECM is analyzed for its content (expression) of collagen types I and III, fibronectin, small leucine-rich proteoglycans (e.g. biglycan and decorin), and major basement membrane components (e.g. perlecan and laminin). In addition, stem cell proliferation and SSEA-4 expression are routinely examined for each new batch of ECM. Although donor-to-donor variation between batches of ECM may not be completely mitigated by this standardized approach, the effects of the ECM on cell behavior display similar trends.

### Assessment of cell proliferation on the culture surfaces

BM- and AD-MSCs, as well as HeLa, MCF7 and MDA-MB-231 cancer cell lines (kindly provided by Dr. Rong Li, Department of Molecular Medicine, UTHSCSA) were seeded on BM-ECM, AD-ECM, and TCP at 2000 cells/cm$^2$. MSCs were cultured for 4 days in "growth media" (see above), while the cancer cells were cultured for 4 days in high-glucose DMEM (Life Technologies, Grand Island, NY) supplemented with penicillin (100 U/mL), streptomycin (100 μg/mL) (Sigma-Aldrich) and 10% FBS. At harvest, cells were released from the culture surfaces and counted. Cells cultured on ECM surfaces were incubated for 10 min at 37 °C with collagenase (400 U/mL; Type II, Worthington Biochemical Inc., Lakewood, NJ), while those cultured on TCP were incubated with trypsin. The released cells were collected, washed with PBS, and then counted using a hemocytometer and trypan blue staining. Proliferation experiments were performed at least three times using an n = 3 for each treatment group. The data shown are the mean ± 95% confidence interval.

### Assessment of cell spreading morphology on the culture surfaces

BM- and AD-MSCs were seeded on BM-ECM, AD-ECM, and TCP at 2000 cells/cm $^2$ and cultured for 24 h in growth media. At 24 h, the cells on each substrate were imaged using an IX73 inverted bright field microscope (Olympus Corp., Center Valley, PA) at 4 × magnification. Single cells were selected (within the field of view) and then outlined using cellSens Dimension software (Olympus Corp., Center Valley, PA). Circularity ($C$) was computed as a ratio of measured cell area ($A_{cell}$, μM $^2$) to perimeter ($P_{cell}$, μM) according to the relationship:

$$C = \frac{A_{\Pi} A_{cell}}{P_{cell}^2}$$

such that as the circularity value approaches "1" for cells of idealized circularity. Cell circularity data represents the mean ± 95% confidence interval of 76 randomly-selected cells from 2.190 mm × 1.648 mm areas of each of the culture substrates.

### Assay of osteoblast (OB) and adipocyte (AD) differentiation efficiency of BM-MSCs cultured on the different surfaces

BM-MSCs were seeded on BM-ECM, AD-ECM, and TCP at 6 × 10 $^3$ cells/cm $^2$ and cultured for 14 days in growth media. At day 7, to assess the adipogenic differentiation efficiency of the cells, cultures were transferred to adipogenic media (DMEM containing 10% FBS, 0.5 mM IBMX, $10^{-6}$ M dexamethasone, 10 μM insulin, and 200 μM

indomethacin), maintained for an additional 10 days, fixed with 10% formalin for 1 h at room temperature, and then stained with Oil Red O. To assess osteogenic differentiation efficiency, the cultures were transferred to osteoblast differentiation media (growth media supplemented with $10^{-7}$ M dexamethasone [Sigma-Aldrich, St. Louis, MO] and $10^{-4}$ M L-ascorbate-2-phosphate [Wako Chemicals, Richmond, VA]), maintained an additional 25 days, fixed with 10% formalin for 1 h at room temperature, and then stained with Alizarin Red [75]. For each condition, 15 randomly selected areas in each of three wells were imaged at 4 × magnification. Differentiation efficiency was calculated (ratio of OB- or AD-stained pixels to methyl violet pixels in the baseline cultures) by pixel quantitation using binary image analysis performed in ImageJ (NIH, Bethesda, MD). Differentiation efficiency data points represent the mean ± 95% confidence interval of 15 randomly-selected (0.876 mm × 0.659 mm) areas on BM-, AD-ECM and TCP. Each experiment was repeated a minimum of three times.

### Compositional analysis of BM- and AD-ECM using mass spectrometry

Proteins were separated by 1-D SDS-PAGE and stained with Coomassie blue. Bands of interest were excised and the proteins digested *in situ* with trypsin (Promega, modified). The digests were analyzed by capillary HPLC-electrospray ionization tandem mass spectrometry (HPLC-ESI-MS/MS) on a Thermo Fisher LTQ fitted with a New Objective PicoView 550 nanospray interface. On-line HPLC separation of the digests was accomplished with an Eksigent NanoLC micro HPLC. A mass spectral scan strategy was used in which a survey scan was acquired followed by data-dependent collision-induced dissociation (CID) spectra of the seven most intense ions in the survey scan. Mascot (Matrix Science) was used to search the mass spectra searched against the SwissProt database. Methionine oxidation was considered as a variable modification. Cross correlation of the Mascot results with X! Tandem and determination of protein and peptide identity probabilities were accomplished by Scaffold (Proteome Software). Protein identifications were accepted using the following criteria: minimum number of peptides, 2; peptide probability, ≥ 95%; protein probability, ≥ 99%.

### Second-harmonic generation (SHG) imaging of BM- and AD-ECM

BM- and AD-ECM were rehydrated by washing twice with $ddH_2O$ and then incubating in PBS for 1 h at 37 °C. Following incubation, the ECM samples were washed again and transferred to $ddH_2O$ for imaging. Second-harmonic generation (SHG) imaging was performed using a Prairie Technologies Ultima multiphoton imaging system (Bruker, Madison, WI) equipped with a Nikon FN-1 upright microscope and a Nikon Apo LWD 25X (N.A. 1.1) immersion objective. The excitation wavelength (800 nm) was generated by a Chameleon Ultra II femtosecond pulse laser (Coherent Inc., Santa Clara, CA). Using a backward detection scheme, the SHG signal was collected with a non-descanned photomultiplier tube with a 417/60 bandpass filter (Semrock Inc., Rochester, NY).

### Immunofluorescent (IF) staining of BM- and AD-ECM

BM- and AD-ECM were rehydrated by incubation in PBS for 1 h at 37 °C and then treated with DNase (100 units/mL; Sigma-Aldrich) for 1 h at 37 °C. After removal of the enzyme and a brief rinse in PBS, the ECMs were fixed with 4% paraformaldehyde/PBS (Sigma-

Aldrich) for 30 min at room temperature. After fixation, the ECMs were washed three times with PBS and then stored in PBS until commencing the staining procedure.

For IF staining, ECMs were first treated with blocking solution (Bloxall, Vector Labs, Inc., Burlingame, CA) for 30 min at room temperature and then incubated for 1 h at 4 °C with primary antibody specific for human type VI collagen (1:200 dilution; polyclonal rabbit IgG; EMD Millipore, Temecula, CA). Non-specific rabbit IgG (Sigma-Aldrich) was employed as a negative control (1:200). Unbound primary antibody was removed by washing with cold (4 °C) PBS. After washing, the ECMs were incubated with blocking solution again for 10 min at room temperature. Secondary antibody (1:200; FITC-conjugated goat anti-rabbit IgG, Sigma-Aldrich) was then added and the incubation continued for 1 h at 4 °C. Florescence microscopy was performed at 10 × magnification using an Olympus IX73 inverted microscope.

### Surface characterization of BM-, AD-ECM and TCP

Surface mapping of BM-, AD-ECM and TCP was performed using a Veeco MultiMode atomic force microscope (AFM) (Bruker, Santa Barbara, CA) in tapping mode. AFM was performed on non-hydrated ECMs. Fiber orientation was quantified in ImageJ using the OrientationJ directional analysis plug-in (Swiss Federal Institute of Technology in Lausanne, EPFL; Switzerland). ImageJ outputs a frequency of tangents to fibers in 180 bins. Each image was rotated such that the mode was 90 degrees and the MATLAB distribution toolbox was used to determine the parameters of a normal distribution that would describe the probability distribution with 95% confidence.

Mean average roughness ($R_a$) of the surfaces was performed using NanoScope software (Bruker, Santa Barbara, CA). Three replicates of each surface were evaluated and 15 randomly selected areas were measured in each. Surface roughness data represents the mean ± 95% confidence interval of 15 randomly-selected areas from BM- and AD-ECM.

### Mechanical characterization of BM- and AD-ECM

The mechanical properties of BM-ECM and AD-ECM were measured using small angle oscillatory shear rheology (SAOS). ECMs were rehydrated by incubation in PBS for 1 h at 37 °C. SAOS was performed on hydrated ECMs using an MCR 302 Rheometer (Anton Paar, Austria) and testing accomplished using a 25 mm diameter parallel-plate accessory at 37 °C. The head was lowered into contact with the ECM surface using normal-force detection (10 mN). First, amplitude sweeps were performed on each of the ECMs (n = 4) from the 0.25%-25% shear strain range at a constant angular frequency of 10 rad/s. Linear Viscoelastic Regime (LVR) for each ECM was identified from the amplitude sweeps and 0.5% strain as representative of the LVR. Frequency sweeps (n = 4) were performed in the 0.1–100 rad/s range at 0.5% constant strain. Data points represent the mean ± 95% confidence interval of four ECM samples.

### Aqueous contact angle and surface free energy analysis of BM-, AD-ECM, and TCP

A static contact angle analyzer (VCA Optima, AST Products, Inc., Billerica, MA) was used to perform sessile drop goniometry. The measurements were performed on an air-cushioned

table using a high--resolution digital camera (D300S, Nikon GmbH, Düsseldorf, Germany) with macro bellows (PB-4; Nikon) to capture the images. Samples (1 μL) of two polar liquids, dd$H_2O$ and glycerol (≥ 99%, Sigma-Aldrich), and one non-polar liquid, toluene (≥ 99%, Sigma-Aldrich), were pre-equilibrated to room temperature, placed onto the surfaces (BM-ECM, AD-ECM, and TCP) and imaged. Goniometry was performed on dry E CMs. Contact angle measurements for each probe liquid (n = 8) on the three substrates was performed by image analysis in Image J using the DropSnake plug-in (EPFL). The surface free energy of the three substrates was determined using the Oss–Chaudhury–Good thermodynamic approach [23,76]. Individual surface energy components $\left(Y_S^{LW}, Y_S^+, Y_S^-\right)$ of the substrates were computed using Young's Equation:

$$\frac{1+\cos\theta}{2} Y_L = \sqrt{Y_S^{LW} Y_L^{LW}} + \sqrt{Y_S^+ Y_L^-} + \sqrt{Y_S^- Y_L^+}$$

where θ is the measured contact angle and $\left(Y_L^{LW}, Y_L^+, Y_L^-\right)$ are known surface tension parameters of the probe liquid. $Y_L^{LW}$ is the Lipschitz-van der Waals free energy component, $Y_L^+$ is the electron-acceptor component and $Y_L^-$ is the electron-donor component of the probe liquid. Total surface free energy was computed according to the relationship:

$$Y_S^{Total} = Y_S^{LW} + 2\sqrt{Y_S^+ Y_S^-}$$

where $Y_S^{Total}$ Total is the total surface free energy of the substrate. The surface energy data points represent the mean ± 95% confidence interval of eight independent measurements of contact angle for each of the three probe liquids on the substrates.

### Statistical interpretation of data

Statistical analysis was used to compare the response (i.e. proliferation, spreading morphology, differentiation) of an individual cell-type to culture on the different substrates. For this purpose, we employed Student's t-test to determine significance and included a Bonferonni correction to account for multiple comparisons (α = 0.0167). Surface characterization experiments compared properties of BM-, AD-ECM and TCP and thus also utilized the same statistical approach. See above sections for descriptions of individual studies.

## Acknowledgments

This study was supported by a VA Merit Review (1I01BX002145-01) to X-D Chen. We gratefully acknowledge Dr. Rong Li, Department of Molecular Medicine, University of Texas Health Science Center at San Antonio (UTHSCSA), for the kind gift of the HeLa, MCF7 and MDA-MB-231 cancer cell lines and guidance on their maintenance in culture. Mass spectrometry analyses were conducted in the UTHSCSA Institutional Mass Spectrometry Laboratory; the expert technical assistance of Kevin Hakala, M.S. is gratefully acknowledged. This work was supported in part by an NIH shared instrumentation grant (1 S10 RR021160-01) to Dr. Susan T. Weintraub, Director of the Mass Spectrometry Core Laboratory.

## References


[1]. Witkowski JA Dr. Carrel's immortal cells. Med. Hist. 1980; 24:129–142. [PubMed: 6990125]

[2]. Sanford KK, Earle WR. The growth in vitro of single isolated tissue cells. J. Natl. Cancer Inst. 1948; 9:229–246. [PubMed: 18105872]

[3]. Eagle H. Nutrition needs of mammalian cells in tissue culture. Science. 1955; 122:501–514. [PubMed: 13255879]

[4]. Amstein H. Adaptation of plastic surfaces for tissue culture by glow discharge. J. Clin. Microbiol. 1975; 2:46–54. [PubMed: 818106]

[5]. Baker M. Stem cells in culture: defining the substrate. Nat. Methods. 2011; 8:293–297.

[6]. Marx V. Where stem cells call home. Nat. Methods. 2013; 10:111–115. [PubMed: 23361089]

[7]. Lutolf M, Gilbert P, Blau H. Designing materials to direct stem-cell fate. Nature. 2009; 462:433–441. [PubMed: 19940913]

[8]. Behonick DJ, Werb Z. A bit of give and take: the relationship between the extracellular matrix and the developing chondrocyte. Mech. Dev. 2003; 120:1327–1336. [PubMed: 14623441]

[9]. Mott J, Werb Z. Regulation of matrix biology by matrix metalloproteinases. Curr. Opin. Cell Biol. 2004; 16:558–564. [PubMed: 15363807]

[10]. Bi Y, Stuelten C, Kilts T, Wadhwa S, Iozzo R, et al. Extracellular matrix proteoglycans control the fate of bone marrow stromal cells. J. Biol. Chem. 2005; 280:30481–30489. [PubMed: 15964849]

[11]. Chen X. Extracellular matrix provides an optimal niche for the maintenance and propagation of mesenchymal stem cells. Birth defects Res. 2010; 90:45–54. Part C.

[12]. Chen X, Dusevich V, Feng J, Manolagas S, Jilka R. Extracellular matrix made by bone marrow cells facilitates expansion of marrow-derived mesenchymal progenitor cells and prevents their differentiation into osteoblasts. J. Bone Miner. Res. 2007; 22:1943–1956. [PubMed: 17680726]

[13]. Lai Y, Sun Y, Skinner C, Son E, Lu Z, Tuan R, et al. Reconstitution of marrow-derived extracellular matrix ex vivo: a robust culture system for expanding large-scale highly functional human mesenchymal stem cells. Stem Cells Dev. 2010; 19:1095–1107. [PubMed: 19737070]

[14]. Chen XD, Fisher LW, Robey PG, Young MF. The small leucine-rich proteoglycan biglycan modulates BMP-4-induced osteoblast differentiation. FASEB J. 2004; 18:948–958. [PubMed: 15173106]

[15]. Ahmed N, Riley C, Rice G, Quinn M. Role of integrin receptors for fibronectin, collagen and laminin in the regulation of ovarian carcinoma functions in response to a matrix microenvironment. Clin. Exp. Metastasis. 2005; 22:391–402. [PubMed: 16283482]

[16]. Philp D, Chen SS, Fitzgerald W, Orenstein J. Complex extracellular matrices promote tissue-specific stem cell differentiation. Stem Cells. 2005; 23:288–296. [PubMed: 15671151]

[17]. Gleizes PE, Munger JS, Nunes I, Harpel JG. TGF-β latency: biological significance and mechanisms of activation. Stem Cells. 1997; 15:190–197. [PubMed: 9170210]

[18]. Tufvesson E, Westergren-Thorsson G. Tumour necrosis factor-α interacts with biglycan and decorin. FEBS Lett. 2002; 530:124–128. [PubMed: 12387878]

[19]. Nili N, Cheema AN, Giordano FJ, Barolet AW. Decorin inhibition of PDGF-stimulated vascular smooth muscle cell function: potential mechanism for inhibition of intimal hyperplasia after balloon angioplasty. Am. J. Pathol. 2003; 163:869–878. [PubMed: 12937128]

[20]. Hildebrand A, Romarís M, Rasmussen LM, Heinegård D, Twardzik DR, Border WA, et al. Interaction of the small interstitial proteoglycans biglycan, decorin and fibromodulin with transforming growth factor beta. Biochem. J. 1994; 302:527–534. [PubMed: 8093006]

[21]. Santra M, Reed CC, Iozzo RV. Decorin binds to a narrow region of the epidermal growth factor (EGF) receptor, partially overlapping but distinct from the EGF-binding epitope. J. Biol. Chem. 2002; 277:35671–35681. [PubMed: 12105206]

[22]. Chen XD, Shi S, Xu T, Robey PG. Age-related osteoporosis in biglycan-deficient mice is related to defects in bone marrow stromal cells. J. Bone Miner. Res. 2002; 17:331–340. [PubMed: 11811564]

[23]. Oss VC, Chaudhury MK, Good RJ. Monopolar surfaces. Adv. Colloid Interface Sci. 1987; 28:35–64. [PubMed: 3333137]

[24]. Taylor, M. A History of Cell Culture. In: Taylor, M., editor. Viruses and Man: A History of Interactions. Springer International, Cham; Switzerland: 2014. p. 41-52.

[25]. Carrel A, Baker LE. The chemical nature of substances required for cell multiplication. J. Exp. Med. 1926; 44:503–521. [PubMed: 19869202]

[26]. He F, Chen X, Pei M. Reconstruction of an in vitro tissue-specific microenvironment to rejuvenate synovium-derived stem cells for cartilage tissue engineering. Tissue Eng. Part A. 2010; 15:3809–3821.

[27]. Antebi B, Zhang Z, Wang Y, Lu Z, Chen XD, Ling J. Stromal-cell-derived extracellular matrix promotes the proliferation and retains the osteogenic differentiation capacity of mesenchymal stem cells on three-dimensional scaffolds. Tissue Eng. Part C. 2014; 21:171–181.

[28]. Kilian K, Bugarija B, Lahn B, Mrksich M. Geometric cues for directing the differentiation of mesenchymal stem cells. Proc. Natl. Acad. Sci. 2010; 107:4872–4877. [PubMed: 20194780]

[29]. Mathieu P, Loboa E. Cytoskeletal and focal adhesion influences on mesenchymal stem cell shape, mechanical properties, and differentiation down osteogenic, adipogenic, and chondrogenic pathways. Tissue Eng. Part B. 2012; 18:436–444.

[30]. Treiser M, Yang E, Gordonov S, Cohen D, Androulakis I, Kohn J, et al. Cytoskeleton-based forecasting of stem cell lineage fates. Proc. Natl. Acad. Sci. 2010; 107:610–615. [PubMed: 20080726]

[31]. Sadie-Van Gijsen H, Crowther NJ, Hough FS, Ferris WF. The interrelationship between bone and fat: from cellular see-saw to endocrine reciprocity. Cell. Mol. Life Sci. 2012; 70:2331–2349. [PubMed: 23178849]

[32]. Curran JM, Chen R, Hunt JA. Controlling the phenotype and function of mesenchymal stem cells in vitro by adhesion to silane-modified clean glass surfaces. Biomaterials. 2005; 26:7057–7067. [PubMed: 16023712]

[33]. Ghosh S, Ashcraft K, Jahid M, April C, Ghajar CM, Ruan J, et al. Regulation of adipose oestrogen output by mechanical stress. Nat. Commun. 2013; 4:1821. [PubMed: 23652009]

[34]. Nagelkerke A, Bussink J, Rowan AE, Span PN. The mechanical microenvironment in cancer: how physics affects tumours. Semin. Cancer Biol. 2015; 35:62–70. [PubMed: 26343578]

[35]. Kalamajski S, Oldberg A. The role of small leucine-rich proteoglycans in collagen fibrillogenesis. Matrix Biol. 2010; 29:248–253. [PubMed: 20080181]

[36]. Kresse H, Schönherr E. Proteoglycans of the extracellular matrix and growth control. J. Cell. Physiol. 2001; 189:266–274. [PubMed: 11748584]

[37]. Reese S, Underwood C, Weiss J. Effects of decorin proteoglycan on fibrillogenesis, ultrastructure, and mechanics of type I collagen gels. Matrix Biol. 2013; 32:414–423. [PubMed: 23608680]

[38]. Iwasaki S, Hosaka Y, Iwasaki T, Yamamoto K, Nagayasu A, Ueda H, et al. The modulation of collagen fibril assembly and its structure by decorin: an electron micro-scopic study. Arch. Histol. Cytol. 2008; 71:37–44. [PubMed: 18622092]

[39]. Raspanti M, Viola M, Sonaggere M, Tira M, Tenni R. Collagen fibril structure is affected by collagen concentration and decorin. Biomacromolecules. 2007; 8:2087–2091. [PubMed: 17530890]

[40]. Orgel JP, Irving TC, Miller A, Wess TJ. Microfibrillar structure of type I collagen in situ. Proc. Natl. Acad. Sci. 2006; 103:9001–9005. [PubMed: 16751282]

[41]. Bidanset DJ, Guidry C, Rosenberg LC, Choi HU, Timpl R, Hook M. Binding of the proteoglycan decorin to collagen type VI. J. Biol. Chem. 1992; 267:5250–5256. [PubMed: 1544908]

[42]. Wiberg C, Hedbom E, Khairullina A, Timpl R, et al. Biglycan and decorin bind close to the n-terminal region of the collagen VI triple helix. J. Biol. Chem. 2001; 276:18947–18952. [PubMed: 11259413]

[43]. Wiberg C, Heinegård D, Wenglén C, Timpl R, Mörgelin M. Biglycan organizes collagen VI into hexagonal-like networks resembling tissue structures. J. Biol. Chem. 2002; 277:49120–49126. [PubMed: 12354766]

[44]. Font B, Eichenberger D, Rosenberg LM, Van Der Rest M. Characterization of the interactions of type XII collagen with two small proteoglycans from fetal bovine tendon, decorin and fibromodulin. Matrix Biol. 1996; 15:341–348. [PubMed: 8981330]

[45]. Agarwal P, Zwolanek D, Keene D, Schulz JN, Blumbach K, Heinegård D, et al. Collagen XII and XIV, new partners of cartilage oligomeric matrix protein in the skin extracellular matrix suprastructure. J. Biol. Chem. 2012; 287:22549–22559. [PubMed: 22573329]

[46]. Zhang G, Chen S, Goldoni S, Calder B, Simpson H, Owens R, et al. Genetic evidence for the coordinated regulation of collagen fibrillogenesis in the cornea by decorin and biglycan. J. Biol. Chem. 2009; 284:8888–8897. [PubMed: 19136671]

[47]. Schönherr E, Witsch-Prehm P, Harrach B, Robenek H, Rauterberg J, Kresse H. Interaction of biglycan with type I collagen. J. Biol. Chem. 1995; 270:2776–2783. [PubMed: 7852349]

[48]. Douglas T, Heinemann S, Bierbaum S, Scharnweber D, Worch H. Fibrillogenesis of collagen types I, II, and III with small leucine-rich proteoglycans decorin and biglycan. Biomacromolecules. 2006; 7:2388–2393.

[49]. Iozzo R, Schaefer L. Proteoglycan form and function: a comprehensive nomenclature of proteoglycans. Matrix Biol. 2015; 42:11–55. [PubMed: 25701227]

[50]. Andersen DC, Kortesidis A, Zannettino AC, Kratchmarova I, Chen L, Jensen ON, Teisner B, Gronthos S, Jensen CH, Kassem M. Development of novel monoclonal antibodies that define differentiation stages of human stromal (mesenchymal) stem cells. Mol. Cell. 2011; 32:133–142.

[51]. Urciuolo A, Quarta M, Morbidoni V, Gattazzo F, Molon S, Grumati P, Montemurro F, Tedesco FS, Blaauw B, Cossu G, Vozzi G, Rando TA, Bonaldo P. Collagen VI regulates satellite cell self-renewal and muscle regeneration. Nat. Commun. 2013; 4:1964–1989. [PubMed: 23743995]

[52]. Ross A, Jiang Z, Bastmeyer M, Lahann J. Physical aspects of cell culture substrates: topography, roughness, and elasticity. Small. 2012; 8:336–355. [PubMed: 22162324]

[53]. Lord M, Foss M, Besenbacher F. Influence of nanoscale surface topography on protein adsorption and cellular response. Nano Today. 2010; 5:66–78.

[54]. Mei Y, Saha K, Bogatyrev S, Yang J, Hook A, Kalcioglu I, et al. Combinatorial development of biomaterials for clonal growth of human pluripotent stem cells. Nat. Mater. 2010; 9:768–778. [PubMed: 20729850]

[55]. Jiang J, Papoutsakis E. Stem-cell niche based comparative analysis of chemical and nano-mechanical naterial properties impacting ex vivo expansion and differentiation of hematopoietic and mesenchymal stem cells. Adv. Healthcare Mater. 2013; 2:25–42.

[56]. McMurray R, Gadegaard N, Tsimbouri M, Burgess K, McNamara L, Tare R, et al. Nanoscale surfaces for the long-term maintenance of mesenchymal stem cell phenotype and multipotency. Nat. Mater. 2011; 10:637–644. [PubMed: 21765399]

[57]. Dalby M, Gadegaard N, Tare R, Andar A, Riehle M, Herzyk P, et al. The control of human mesenchymal cell differentiation using nanoscale symmetry and disorder. Nat. Mater. 2007; 6:997–1003. [PubMed: 17891143]

[58]. Olivares-Navarrete R, Hyzy S, Hutton D, Erdman C, Wieland M, Boyan B, et al. Direct and indirect effects of microstructured titanium substrates on the induction of mesenchymal stem cell differentiation towards the osteoblast lineage. Biomaterials. 2010; 31:2728–2735. [PubMed: 20053436]

[59]. Engler A, Sen S, Sweeney L, Discher D. Matrix elasticity directs stem cell lineage specification. Cell. 2006; 126:677–689. [PubMed: 16923388]

[60]. Buxboim A, Ivanovska I, Discher D. Matrix elasticity, cytoskeletal forces and physics of the nucleus: how deeply do cells “feel” outside and in? J. Cell Sci. 2010; 123:297–308. [PubMed: 20130138]

[61]. Discher DE, Janmey P, Wang YLL. Tissue cells feel and respond to the stiffness of their substrate. Science. 2005; 310:1139–1143. [PubMed: 16293750]

[62]. Reilly G, Engler A. Intrinsic extracellular matrix properties regulate stem cell differentiation. J. Bio. Mech. 2010; 43:55–62.

[63]. Tse J, Engler A. Stiffness gradients mimicking in vivo tissue variation regulate mesenchymal stem cell fate. PLoS ONE. 2011; 6:e15978. http://dx.doi.org/10.1371/journal.pone. 0015978. [PubMed: 21246050]

[64]. Eyckmans J, Chen C. Stem cell differentiation: sticky mechanical memory. Nat. Mater. 2014; 13:542–543. [PubMed: 24845990]

[65]. Lecuit T, Lenne PFF. Cell surface mechanics and the control of cell shape, tissue patterns and morphogenesis. Nat. Rev. Mol. Cell Biol. 2007; 8:633–644. [PubMed: 17643125]

[66]. Phillips J, Petrie T, Creighton F, García A. Human mesenchymal stem cell differentiation on self-assembled monolayers presenting different surface chemistries. Acta Biomater. 2009; 6:12–20. [PubMed: 19632360]

[67]. Singhvi R, Kumar A, Lopez GP, Stephanopoulos GN, Wang DI, Whitesides GM, et al. Engineering cell shape and function. Science. 1994; 264:696–698. [PubMed: 8171320]

[68]. Dike L, Chen C, Mrksich M, Tien J, Whitesides G, Ingber D. Geometric control of switching between growth, apoptosis, and differentiation during angiogenesis using micropatterned substrates. Vitro Cell. Dev. Biol. Anim. 1999; 35:441–448.

[69]. Hallab NJ, Bundy KJ, O'Connor K, Moses RL, Jacobs JJ. Evaluation of metallic and polymeric biomaterial surface energy and surface roughness characteristics for directed cell adhesion. Tissue Eng. 2001; 7:55–71. [PubMed: 11224924]

[70]. Kennedy S, Washburn N, Simon C, Amis E. Combinatorial screen of the effect of surface energy on fibronectin-mediated osteoblast adhesion, spreading and proliferation. Biomaterials. 2006; 27:3817–3824. [PubMed: 16563495]

[71]. Zeiger A, Hinton B, Vliet K. Why the dish makes a difference: quantitative comparison of polystyrene culture surfaces. Acta Biomater. 2013; 9:7354–7361. [PubMed: 23454055]

[72]. Zhao G, Raines AL, Wieland M, Schwartz Z, Boyan BD. Requirement for both micron-and submicron scale structure for synergistic responses of osteoblasts to substrate surface energy and topography. Biomaterials. 2007; 28:2821–2829. [PubMed: 17368532]

[73]. Curran J, Chen R, Hunt J. The guidance of human mesenchymal stem cell differentiation in vitro by controlled modifications to the cell substrate. Biomaterials. 2006; 27:4783–4793. [PubMed: 16735063]

[74]. Valamehr B, Jonas S, Polleux J, Qiao R, Guo S, Gschweng E, et al. Hydrophobic surfaces for enhanced differentiation of embryonic stem cell-derived embryoid bodies. Proc. Natl. Acad. Sci. 2008; 105:14459–14464. [PubMed: 18791068]

[75]. Mosna F, Sensebé L, Krampera M. Human bone marrow and adipose tissue mesenchymal stem cells: a user's guide. Stem Cells Dev. 2010; 19:1449–1470. [PubMed: 20486777]

[76]. Xu Z, Liu Q, Ling J. An evaluation of the van Oss– Chaudhury–Good equation and Neumann's equation of state approach with mercury substrate. Langmuir. 1995; 11:1044–1046.

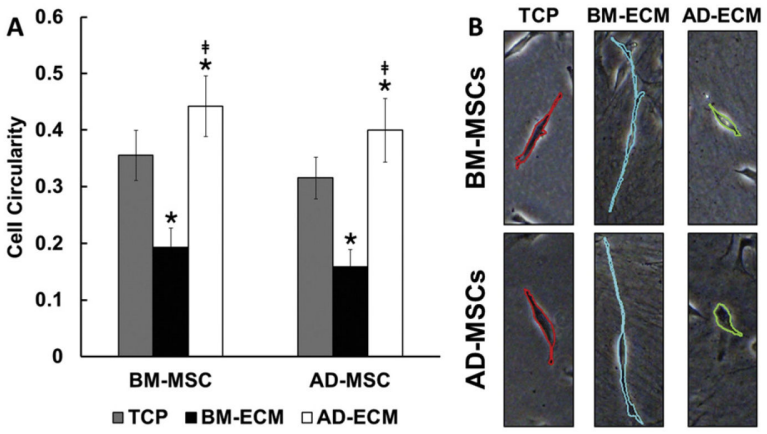


**Fig. 1.**

Proliferation of MSCs and cancer cells on the three different culture substrates. Cells were grown for 4 days on the three culture substrates (TCP, BM-ECM, and AD-ECM), released from the surfaces, and then counted after trypan blue staining. The data are presented as the number of cells per $cm^2$. (A) BM-MSCs or AD-MSCs were cultured on the three substrates. (B) Cancer cell lines were cultured on the three substrates. *P < 0.05, vs. TCP; ***‡P < 0.05, vs. BM-ECM.

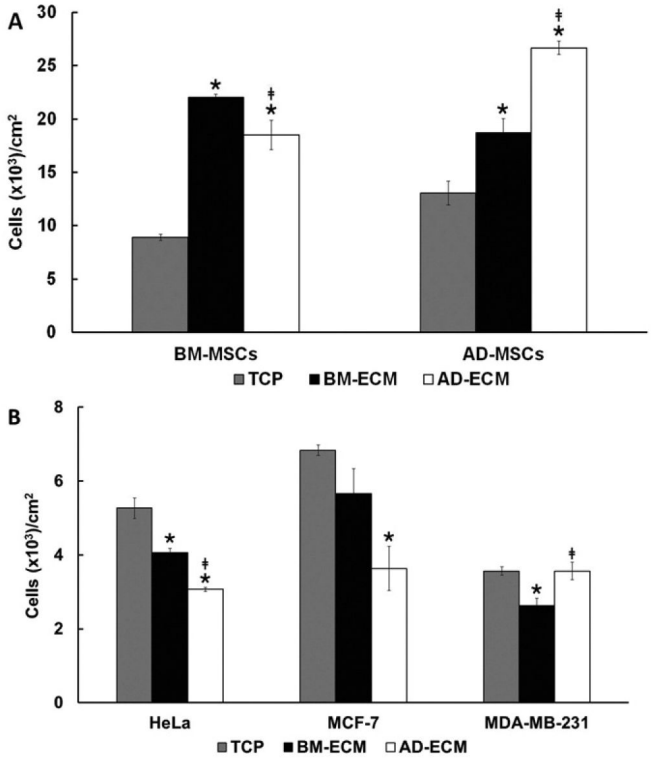


**Fig. 2.**

Culture substrate affected MSC spreading morphology. BM- and AD-MSCs were cultured on TCP, BM-ECM, and AD-ECM for 24 h and spreading morphology measured. (A) Quantification of cell circularity on the various substrates. *P < 0.05, vs. TCP; ‡P < 0.05, vs. BM-ECM. (B) Morphology of the MSCs on the three substrates using brightfield microscopy.

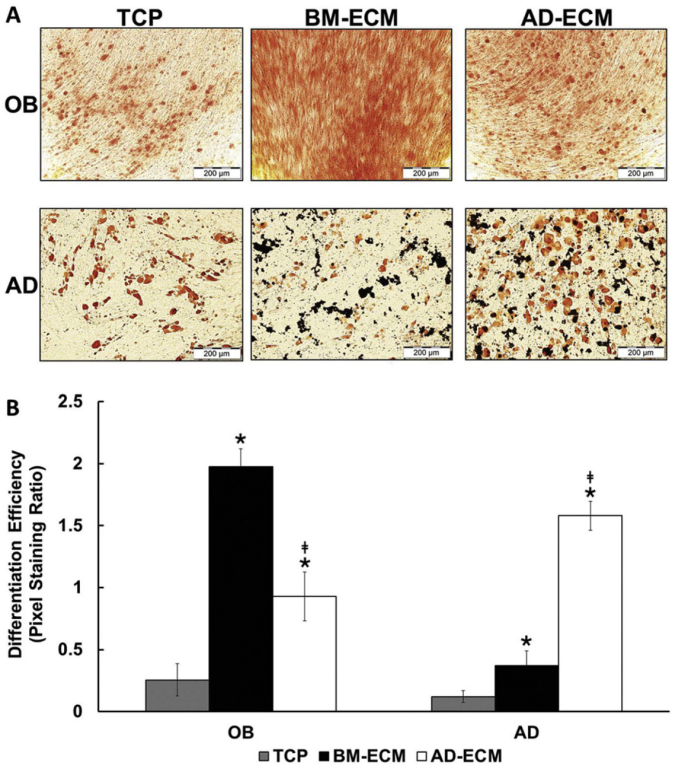


**Fig. 3.**

Osteogenic (OB) and adipogenic (AD) differentiation of BM-MSCs was directed by culture surface. (A) OB differentiation of the BM-MSCs was visualized using Alizarin Red staining for calcification and AD differentiation was visualized using Oil Red O staining for lipid droplets. (B) Quantification of pixel staining, as a measure of differentiation efficiency, was performed on 15 randomly-selected areas for each substrate. *P < 0.05, vs. TCP; ‡P < 0.05, vs. BM-ECM.

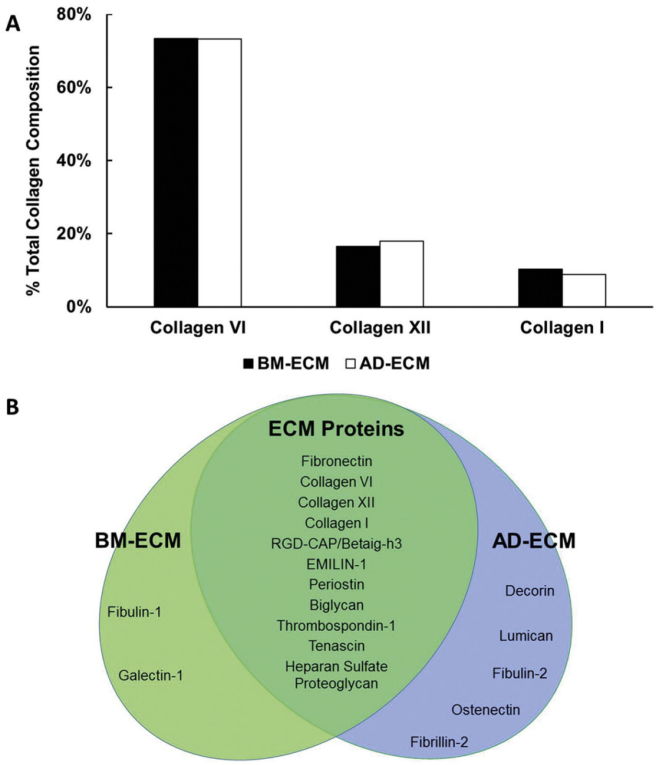


**Fig. 4.**

Protein composition of BM- and AD-ECM determined by mass spectrometric analysis. (A) The principle collagen components of both ECMs were types VI, XII and I. (B) Protein components of BM- and AD-ECM that are shared in common or unique.

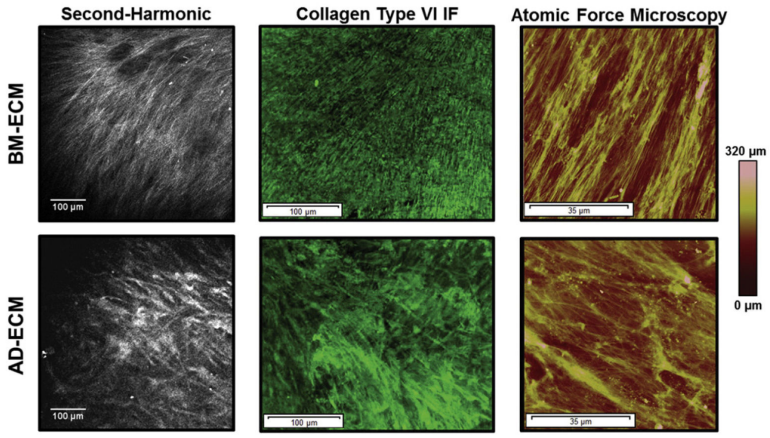


**Fig. 5.**

Principle architectural differences between BM- and AD-ECMs as revealed by microscopic imaging. (A) Second-harmonic generation microscopy, (B) collagen type VI immunofluorescent staining, and (C) atomic force microscopy.

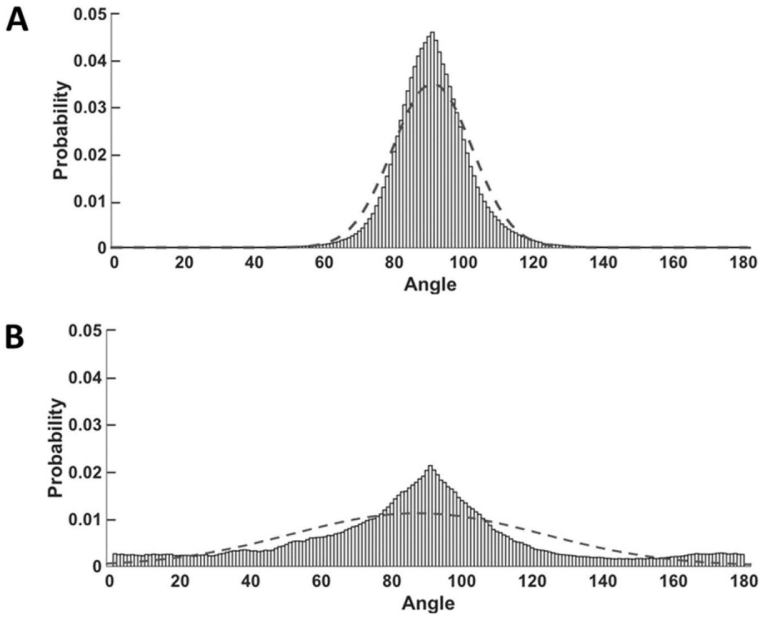


**Fig. 6.**

Fiber orientation differences between BM- and AD-ECMs. Data were fit to a normal distribution, with 90° corresponding to the mode of the observed orientations. The fit-line of the distribution is overlaid on the raw data. (A) Fibrous structures in BM-ECM displayed densely-organized and highly-oriented fibers ($\sigma = 11.3$), while AD-ECM fibers in (B) exhibited a broader range of orientations ($\sigma = 35.6$). Mean fiber orientation measurements were performed on 15 randomly-selected areas of BM- and AD-ECM (70 μM × 70 μM) atomic force microscopy images.

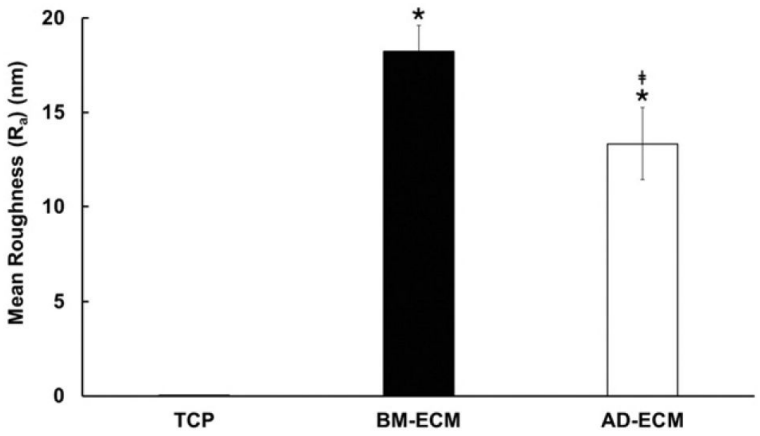


**Fig. 7.**

Surface topography of BM- and AD-ECMs. Measurement of surface roughness ($R_a$) was performed using atomic force microscopy on 15 randomly-selected areas measuring 70 μM × 70 μM. The roughness of TCP was too low to be measured using this method. * $P < 0.05$, vs. TCP; ‡$P < 0.05$, vs. BM-ECM.

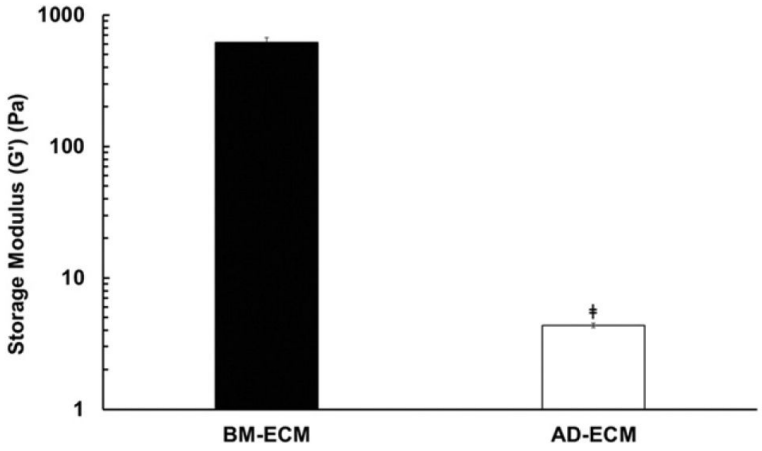


**Fig. 8.**

Mechanical properties of BM- and AD-ECM. Storage modulus was measured by performing four mechanical tests on each ECM using small angle oscillatory shear rheology (SAOS). ‡$P < 0.05$, vs. BM-ECM.

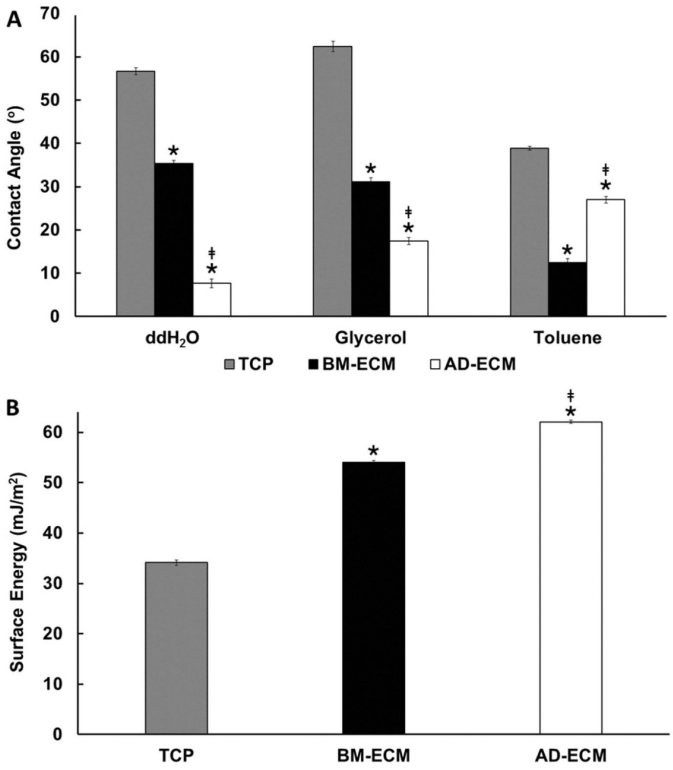


**Fig. 9.**

Aqueous contact angle and surface free energy of TCP, BM-ECM and AD-ECM. (A) Water ($ddH_2O$), glycerol and toluene formed unique contact angles on the three substrates. Data represent 8 measurements for each solvent on each substrate. (B) Oss–Chaudhury–Good analysis revealed considerable differences in surface energy between the three substrates. * $P < 0.05$, vs. TCP; ‡$P < 0.05$, vs. BM-ECM.